AIAA JOURNAL
Vol. 32, No. 3, March 1994

Compressible Navier-Stokes Computations of Multielement Airfoil Flows Using Multiblock Grids

T. E. Nelson,* D. W. Zingg,† and G. W. Johnston‡
University of Toronto, Downsview, Ontario M3H 5T6, Canada

Numerical solutions of the compressible thin-layer Navier-Stokes equations are presented for high-lift multielement airfoil configurations. Multiblock grids are used, allowing straightforward implementation of an approximately factored implicit algorithm. Interfaces between blocks are treated by overlapping the grids and taking one layer of points from neighboring blocks. Turbulence is modeled using the Baldwin-Barth one-equation turbulence model. High-lift applications presented for comparison with wind tunnel data include: an NACA 4412 airfoil with NACA 4415 flap, a GA(W)-1 airfoil with a 29% chord flap at 30-deg flap angle and two gap settings, and a GA(W)-1 airfoil with 15% chord slat and 29% chord flap. Good agreement with experimental data is obtained for cases with fully attached flow or small regions of separated flow. For cases with extensive regions of flow separation, the thickness and extent of the separated regions are underpredicted.

Nomenclature

c	= chord length
C_D	= drag coefficient
C_L	= lift coefficient
C_M	= pitching moment coefficient
C_p	= pressure coefficient
G	= gap
M	= Mach number
O	= overlap
p	= pressure
Re	= Reynolds number
x, y	= Cartesian coordinates
α	= angle of attack
δ	= deflection angle

Subscripts

f	= flap
m	= main airfoil
s	= slat

Introduction

THE flow around two-dimensional high-lift configurations is complex, often containing multiple separated regions and confluent boundary layers. Compressibility effects can also be important even at low-onset flow speeds. Thus, the performance of high-lift devices can be difficult to predict. Codes that couple the boundary-layer and inviscid solutions have been used for many years.[1,2] However, such codes do not model the full range of complex flow features encountered. Consequently, several computational methods for solving the Navier-Stokes equations for multielement airfoil flows have recently been reported in the literature.[3–7] Since a single structured grid cannot be generated about a multielement geometry, multiple structured grids[3–5,7] and unstructured grids[6] have been used. The multiple structured grids can be either patched, as in the multiblock approach,[3,5,7] or overlapped, as in the Chimera approach.[3,4]

For complex turbulent flows, the choice of turbulence model can have a large impact on accuracy and computational expense. Simple algebraic models, such as the Baldwin-Lomax model,[8] have been used extensively for single-element airfoil computations. Although such models have been quite successful, especially when the flow is attached, and have been used for computation of multielement cases as well,[3–7] they are not well suited for some of the phenomena that occur in the multielement case. Turbulence models that include partial differential equations governing the transport of either scalar turbulence parameters or the turbulent stresses are potentially more accurate for complex flows. In a scale evolution model, the turbulent stresses are determined from the local mean flowfield and a number of scalar turbulent parameters, usually through the eddy viscosity approximation. The most popular example of such a model is the k-ε model, used by Mavriplis[9] for multielement airfoil computations. One-equation scale evolution models have recently been presented in Refs. 10 and 11. These models are more robust and easier to implement than the k-ε model but their range of application is not yet well known. There is some evidence that the eddy viscosity approximation may be inaccurate for wake-boundary layer interactions and large separations. In particular, Squire[12] found that the strong interaction of the near wake of a slat with the main airfoil boundary layer may result in "negative eddy viscosity." This phenomenon cannot be modeled using the eddy viscosity concept. Such effects are local, however, and therefore one- and two-equation models can be sufficiently accurate for many applications.

In this paper, steady-state solutions of the compressible thin-layer Navier-Stokes equations for several high-lift multielement airfoil configurations are presented. The approximately factored implicit algorithm used in the well-established Navier-Stokes code ARC2D has been extended for use with multiple blocks. Although this algorithm is not the fastest for steady-state computations,[13] its performance can be enhanced using multigrid.[14] Furthermore, the algorithm is well suited for time-accurate computations of viscous flows. Although the present applications are steady, many flows over high-lift configurations are unsteady, especially near stall or poststall. Turbulence is modeled using the Baldwin-Barth one-equation turbulence model. Extensive comparisons are made with experimental data, hence the results provide a useful assessment of the turbulence model for this class of flows.

Numerical Algorithm

The solution method used here for the thin-layer Navier-Stokes equations is an adaptation of the diagonal form of the Beam and Warming implicit approximate factorization algorithm in generalized coordinates, as used in the code ARC2D. Spatial derivatives are approximated using second-order centered differences. The solution is advanced in time using implicit Euler time-marching, and local time stepping is used to accelerate convergence. A nonlinear artificial dissipation model with second- and fourth-difference dis-

Received March 19, 1993; revision received Aug. 12, 1993; accepted for publication Aug. 21, 1993. Copyright © 1993 by the American Institute of Aeronautics and Astronautics, Inc. All rights reserved.

*Research Assistant, Institute for Aerospace Studies.
†Associate Professor, Institute for Aerospace Studies.
‡Professor, Institute for Aerospace Studies.

sipation terms is used to control oscillations and nonlinear instability. The inviscid portion of the equations is diagonalized so only scalar pentadiagonal systems of equations are solved at each time step.

On a multiblock grid, each block is solved independently. One row of halo points is used in each block to store information from neighboring blocks and intermediate quantities are passed between blocks as required. Interfaces between blocks are treated either by overlapping the grids or averaging the values of neighboring points. Grids are generated using the automated procedure presented in Ref. 15.

For comparison with uncorrected wind tunnel data, the wind tunnel walls are included in the computations. The boundary layer at the tunnel wall is not of interest, so inviscid boundary conditions are applied there. For the wind tunnel outflow boundary, the pressure is adjusted until the average of the upper and lower wall pressures just downstream of the inlet is p_∞. For more information about the numerical method the reader is referred to Refs. 16 and 17.

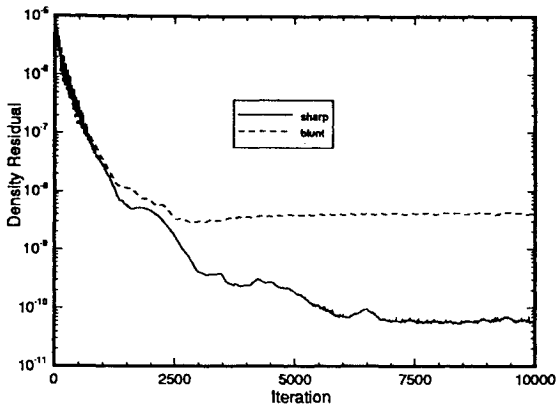

Fig. 1 Convergence history for Adair and Horne test case of NACA 4412 airfoil with NACA 4415 flap. Results with sharp and blunt trailing edges.

Results

NACA 4412 Airfoil with NACA 4415 Flap

The first case considered is the airfoil and flap experiment of Adair and Horne.[18] The experiment consisted of surface pressure measurements and flowfield measurements of velocity and turbulence quantities using both hot-wire and laser anemometry. The airfoil section was an NACA 4412 with an NACA 4415 flap. The model was positioned at $\alpha = 8.2$ deg, $\delta_f = 21.8$ deg, $G_f = 3.5\%c$, $O_f = 2.8\%c$, and tested at $Re = 1.8 \times 10^6$, $M = 0.09$. Transition was fixed at $x/c = 0.025$ and $x/c = 0.010$ downstream of the pressure minimum on the main airfoil upper and lower surfaces, respectively. On the upper surface of the flap, transition was fixed at $x/c = 0.008$ downstream of the pressure minimum; on the lower surface transition was free.

Since the experimental data used for comparison were not corrected for wind tunnel wall effects, the tunnel walls are included in the computations. The wind tunnel test section extended two chords upstream of the leading edge and three chords downstream, so the computational boundaries were placed at the same locations. Approximately 70,000 points were used for the grid, and the off-wall spacing was set to $2 \times 10^{-5}c$ to ensure that $y^+ < 1$ for the first point off the surface. In initial computations, transition was fixed at the locations specified in the experiment and a laminar separation bubble was predicted on the main airfoil. Unfortunately, the bubble was not stable and was occasionally shed downstream, resulting in an unsteady solution. To obtain steady results, the transition point was moved forward to the leading edge.

The computation was performed for the NACA 4412 and NACA 4415 airfoils with both sharp and blunt trailing edges. For

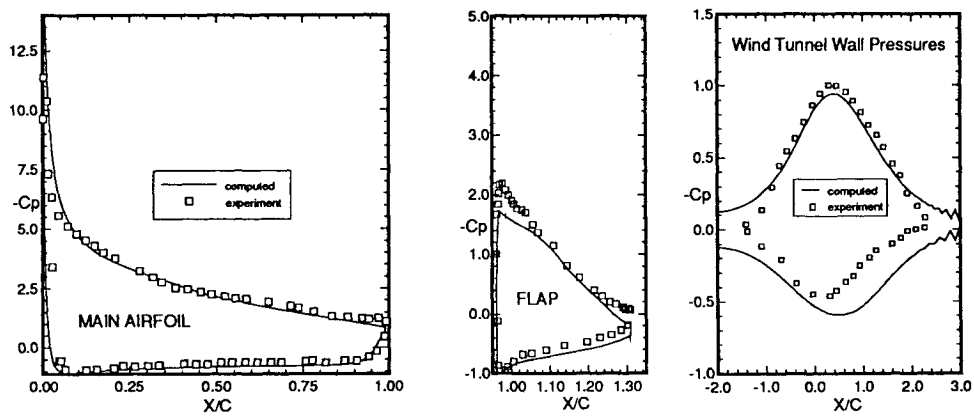

Fig. 2 Surface pressures and wind tunnel wall pressures for Adair and Horne airfoil and flap test case.

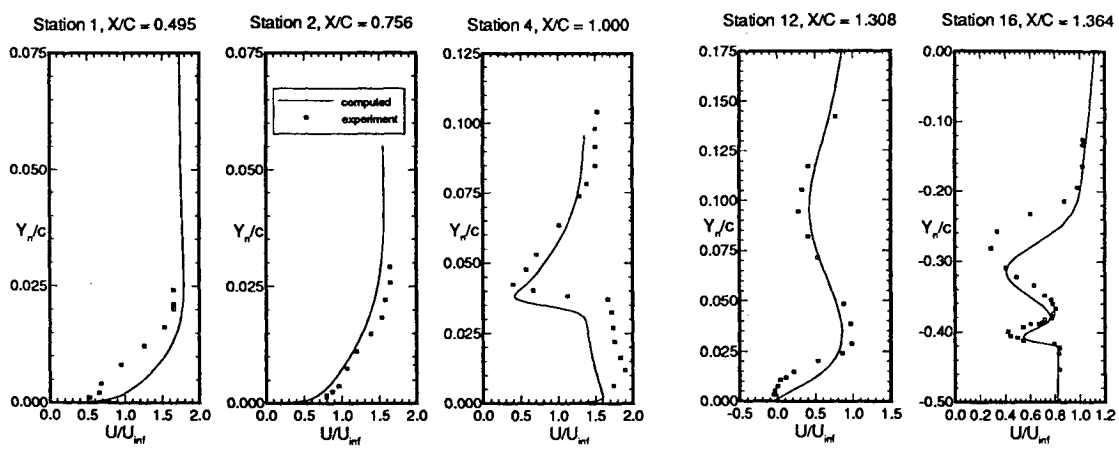

Fig. 3 Comparison of velocity profiles for Adair and Horne airfoil and flap test case.

sharp trailing-edge airfoils, the computation converged very well. With blunt trailing edges, some unsteadiness occurred in the wake region, which prevented complete convergence. A comparison of the convergence history for the two cases is shown in Fig. 1. Differences between the two solutions were small and the following results are for the blunt base airfoils.

A comparison of the pressure distribution with experiment is shown in Fig. 2. The pressure distribution on the flap agrees well with experiment and the flow separates at 87% flap chord, close to the experimentally observed value of 93%. The computed suction peak on the main airfoil is higher than in the experiment and results in additional lift. Wind tunnel wall pressures are shown in the same figure and the agreement is fairly good except near the upstream and the downstream boundaries.

Comparisons of velocity profiles at five stations are shown in Fig. 3. The boundary layer is predicted well on the main airfoil at station 2. At station 1, the agreement is not as good. The flow velocity through the slot, at station 4, is underpredicted but the wake of the main airfoil is predicted fairly well. At the flap trailing edge, station 12, the computed flow has a separated boundary layer profile, but the region of reversed flow is thinner than seen in the experiment. Similar results for profiles and pressure distribution were obtained by Rogers et al.[3] using an incompressible Navier-Stokes solution method with the Baldwin-Barth turbulence model.

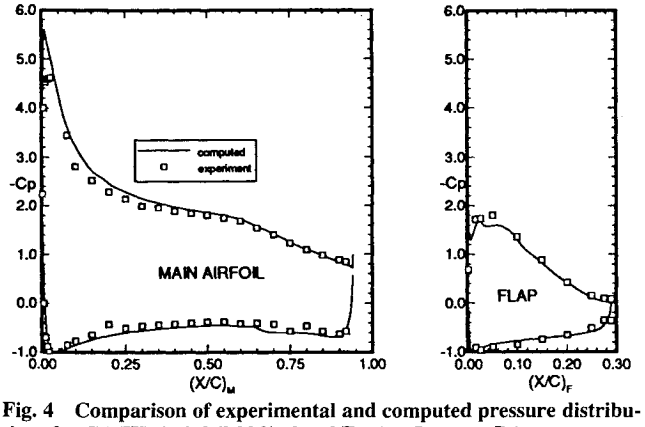

Fig. 4 Comparison of experimental and computed pressure distributions for GA(W)-1 airfoil 29% chord Fowler flap case B4.

GA(W)-1 Airfoil with 29% Chord Fowler Flap

The next case considered is a GA(W)-1 airfoil with a 29% chord Fowler flap. The experimental data are from Braden, Whipkey, Jones, and Lilley, who investigated the flowfield for 25 combinations of flap settings, slat settings, and angles of attack.[19] Included in the experiment were laser velocimeter measurements of velocity profiles, turbulence intensities, and Reynolds shear stresses. Also included were surface pressure measurements, and skin friction and boundary-layer parameters derived from the profiles. The wind tunnel height was 3.33 chords, the upstream boundary was placed 4 chords ahead of the leading edge, and the downstream boundary was placed 5 chords downstream of the leading edge. The off-wall spacing for the grids was again set to $2 \times 10^{-5}c$ to ensure that $y^+ < 1$ for the first point off the surface. Approximately

Table 1 Summary of GA(W)-1 airfoil and flap configurations

Case	α	δ_f	G_f	O_f
B1	3.98	30	4.0	0.0
B2	7.94	30	4.0	0.0
B4	4.13	30	2.5	0.0
B4.5	8.00	30	2.5	0.0

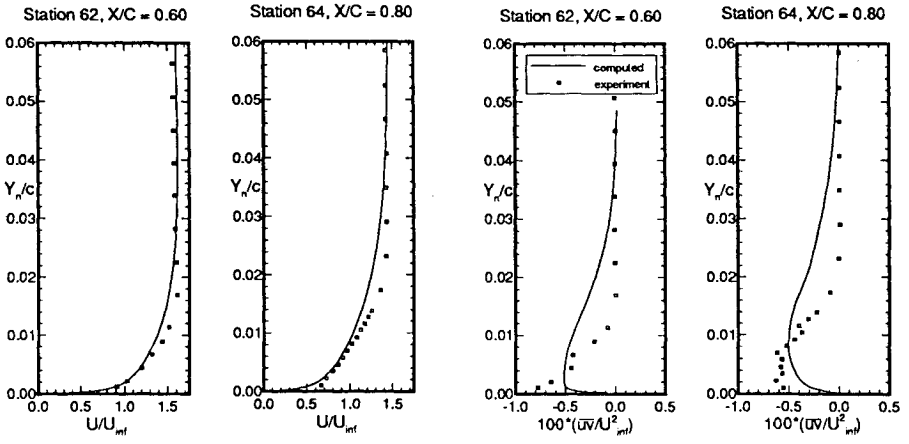

Fig. 5 Boundary layer and Reynolds stress profiles on the upper surface of the main airfoil for the GA(W)-1 airfoil and flap case B4.

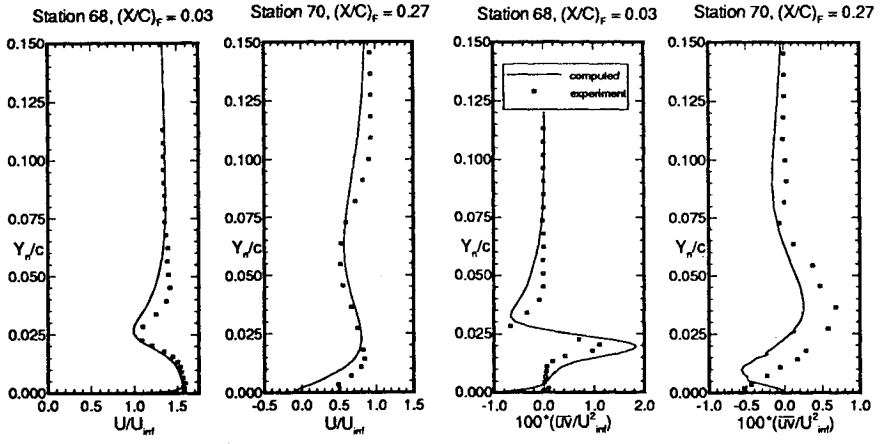

Fig. 6 Boundary layer and Reynolds stress profiles on the upper surface of the flap for the GA(W)-1 airfoil and flap case B4.

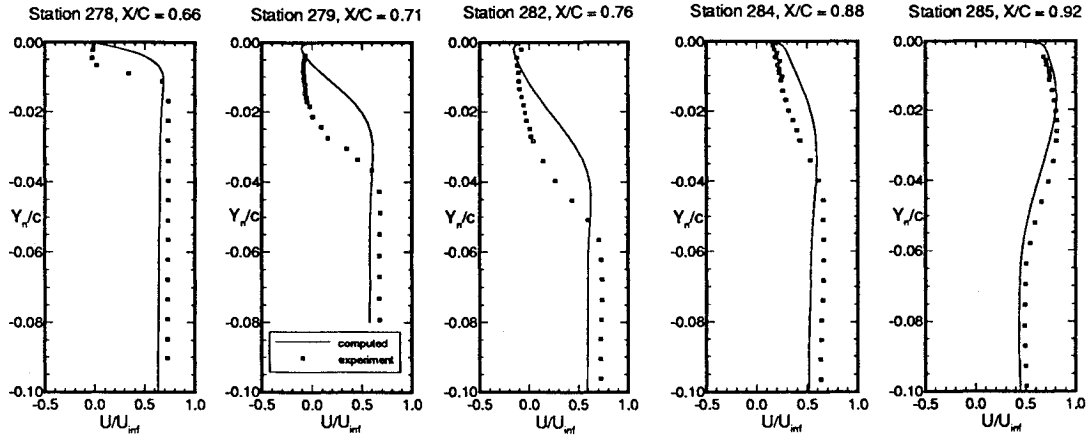

Fig. 7 Boundary layer profiles in the cove region of the main airfoil for GA(W)-1 airfoil and flap case B2.

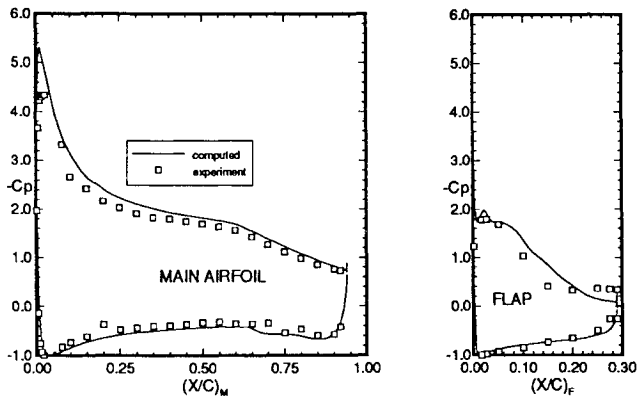

Fig. 8 Comparison of experimental and computed pressure distributions for GA(W)-1 airfoil 29% chord Fowler flap case B1.

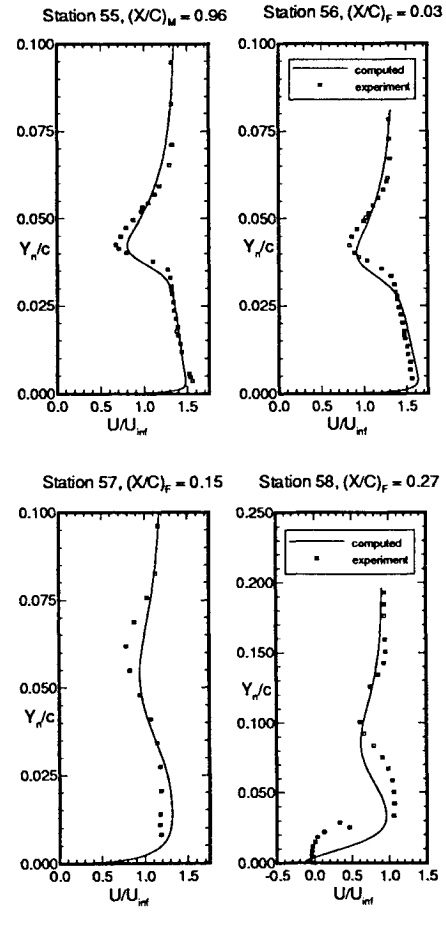

Fig. 9 Boundary layer profiles on the upper surface of the flap for GA(W)-1 airfoil and flap case B1.

60,000 points were used for each grid and typically 20–30 points were included across boundary layer regions.

Experimental test conditions were $Re = 0.62 \times 10^6$ and a stagnation pressure of 20 psf which correspond to $M = 0.116$. The transition was free but was noted to occur naturally at less than 5% chord on the upper surface of the main airfoil and between 50 and 65% chord on the lower surface of the main airfoil. For the computations, the upper surfaces of the main airfoil and flap were assumed to be fully turbulent and transition was set on the lower surfaces at 55% chord on the main airfoil and just ahead of the trailing edge on the flap.

Computations were performed on four airfoil and flap configurations. The cases selected were all $\delta_f = 30$ deg with overlap, $O_f = 0.0\%c$. Angles of attack of $\alpha = 4$ deg and $\alpha = 8$ deg were computed with two gaps, $G_f = 2.5$ and $4.0\%c$. The designations are shown in Table 1. The case with $G_f = 2.5\%c$ and $\alpha = 8$ deg, designated B4.5, was not included in the experiment but was computed here to examine the effect of the gap. For the narrow gap, cases B4 and B4.5, the flow over the flap is fully attached. However, with the wide gap, cases B1 and B2, there is a large separated flow region on the flap.

The computed pressure distribution for case B4 agrees well with experiment, as may be seen in Fig. 4. Boundary layer and Reynolds shear stress profiles for the upper surface of the main airfoil are shown in Fig. 5. The velocity profiles show good agreement, although the Reynolds stress is overpredicted in the outer boundary layer.

On the flap, similar results are obtained for the confluent boundary layer velocity profiles, as shown in Fig. 6. The wake of the main airfoil is captured well as is the development of the flap boundary layer. Near the trailing edge a very small separated region is predicted at station 70, but the experimental profile appears to be attached. Agreement for the Reynolds stress profiles is only fair. In the wake of the main airfoil the magnitude of the Reynolds stress is initially overpredicted but further downstream it is significantly underpredicted.

In all four airfoil and flap computations the separation in the cove region of the main airfoil is significantly underpredicted. An example is shown in Fig. 7 for case B2 which is typical of all four cases. At $x/c = 0.66$, which corresponds to the entrance of the cove, the computed boundary layer profile is attached whereas the experimental profile is separated. Further downstream at $x/c = 0.71$ and 0.76 the computed value of the maximum reversed flow velocity is correct but the bubble is only one-third as thick as in the experiment. After the flow reattaches, the profiles are predicted well as seen at $x/c = 0.92$. This station corresponds to the entrance of the slot and demonstrates that underpredicting the separation in the cove does not dramatically affect the slot flow and hence the flap loading. This agrees with experiments which have demon-

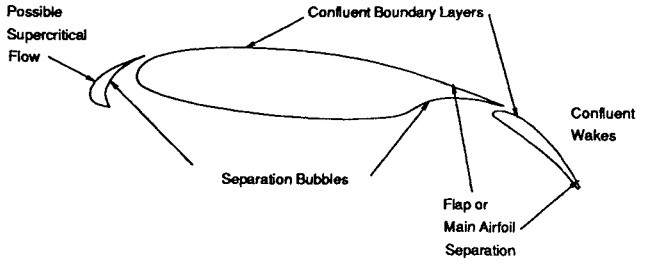

Fig. 10 Flowfield interactions around an airfoil with slat and flap.

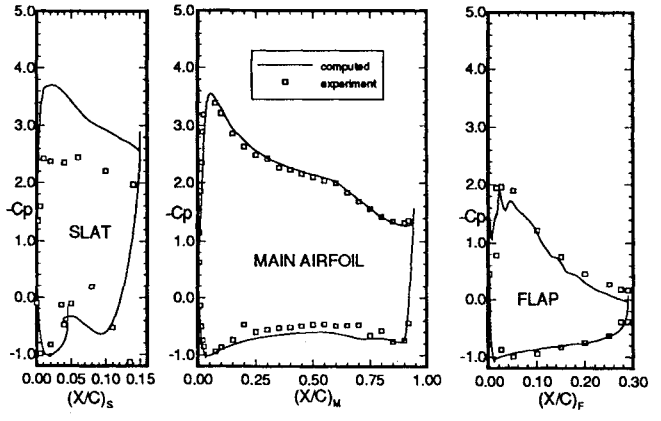

Fig. 11 Comparison of experimental and computed surface pressures for GA(W)-1 airfoil with slat and flap.

strated that high-lift performance is fairly insensitive to cove shape.[20]

For the wide gap cases, there is a large separation on the flap. For case B1, $\alpha = 4$ deg, the flap separation is underpredicted, as shown in Fig. 8. Consequently, the flap carries more load than it should, which in turn increases the loading of the main airfoil. Profiles of the velocity in the confluent boundary layer over the flap are shown in Fig. 9. The main airfoil near wake is captured well but the agreement becomes progressively worse downstream. The flap separation may be seen clearly at station $(x/c)_f = 0.27$. Although the computed profile is separated, the extent of reversed flow is much too small. This result is similar to that seen for the cove separation on the main airfoil. However, high-lift performance is sensitive to flap separation whereas the cove separation is not as significant.

The effect of gap on the lift coefficient is underpredicted because the flap separation is underpredicted. In the experiment, the lift coefficient is reduced by 0.18 as a result of the increased gap. The computations, however, predict a reduction of only 0.05. This discrepancy may be due to the low Reynolds number of the experiment. The turbulence model and thin-layer approximation are intended for high Reynolds numbers, but the experimental Reynolds number was only 0.62×10^6.

GA(W)-1 Airfoil with Slat and Flap

The flowfield about a three-element configuration is considerably more complex than for an airfoil and flap. The leading-edge slat depresses the suction peak on the main airfoil which tends to delay stall. However, the slat wake interacts with the boundary layer on the upper surface of the main airfoil which promotes early boundary layer separation. The merging wakes then interact with the slot flow over the flap. The flow is further complicated by the separation in the cove region of the main airfoil and on the underside of the slat. A diagram of the three-element case is shown in Fig. 10.

The three-element configuration considered here is a GA(W)-1 main airfoil with a 15%c slat at $\delta_s = 42$ deg, $G_s = 1.5\%c$, $O_s = 2.5\%c$, and a 29%c Fowler flap at $\delta_f = 40$ deg, $G_f = 1.5\%c$, and $O_f = 1.5\%c$. The entire configuration is at $\alpha = 5.3$ deg and corresponds to case F-1 of Braden et al.[19] The block decomposition for this case resulted in 31 blocks. A total of 90,000 points were used for the grid and the off-wall spacing was set to $2 \times 10^{-5}c$.

Fig. 12 Streamlines on the lower surface of the slat for the GA(W)-1 airfoil with slat and flap.

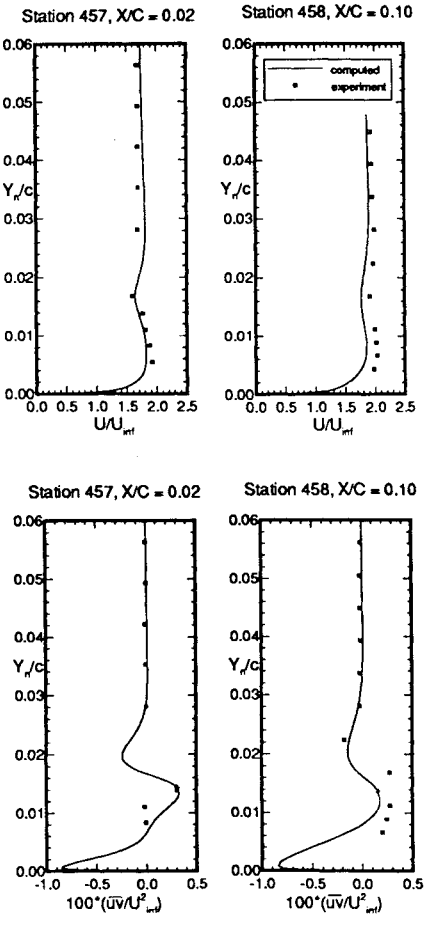

Fig. 13 Velocity and Reynolds stress profiles on the main airfoil for GA(W)-1 airfoil with slat and flap.

A comparison of the computed pressure distribution and experiment is shown in Fig. 11. As may be seen in the figure, the pressure distribution agrees very well for the main airfoil and the flap. For the slat, however, the suction on the upper surface is overpredicted. This result is obtained because the computed separation on the lower surface of the slat is too small. As may be seen from the experimental pressure distribution, stagnation pressure was recorded at 13.5%c. In the computations, however, the reattachment

point is further forward, at 10%c. Therefore, effectively, the slat has more camber, which results in higher loading than seen in the experiment. The details of the computed flow may be seen in Fig. 12, which clearly shows the large separation on the lower surface of the slat and the point of reattachment. The flow is attached at the upper surface trailing edge of both the main airfoil and flap, so the resulting pressure distributions for these elements agree fairly well with experiment. The separation in the cove region of the main airfoil is underpredicted as before.

Comparisons of velocity and Reynolds stress profiles for the upper surface of the main airfoil are shown in Fig. 13. The effect of the merging slat wake on the boundary layer profile is clearly seen in the computations but is not well resolved in the experiment. However, it appears that the wake develops and merges more quickly in the computations than is seen in the experiment.

Conclusions

Numerical solutions of the compressible thin-layer Navier-Stokes equations have been presented for high-lift multielement airfoil configurations. Multiblock grids were used, allowing straightforward implementation of an approximately factored implicit algorithm. Turbulence was modeled using the Baldwin-Barth one-equation turbulence model. Grids were generated with the aid of an automated procedure that divides the domain into blocks.

Good agreement with experiment was obtained when the flow about the configuration was attached or regions of separated flow were small. Computational difficulties encountered included laminar separation bubbles, multiple regions of separated flow, and slightly unsteady flow in wake regions. Results tended to be poor for cases with large regions of separated flow in critical areas such as the flap upper surface or on the slat. Generally, separation points were predicted well, but the extent and thickness of reversed flow regions were underpredicted. The Baldwin-Barth turbulence model worked well in most instances but tended to underpredict eddy viscosity in wake regions and overpredict eddy viscosity in the outer portion of boundary layers.

References

[1]King, D. A., and Williams, B. R., "Developments in Computational Methods for High-Lift Aerodynamics," *Aeronautical Journal*, Vol. 92, No. 917, 1988, pp. 265–288.

[2]Cebeci, T., Chang, K. C., Clark, R. W., and Halsey, N. D., "Calculation of Flow Over Multielement Airfoils at High Lift," *Journal of Aircraft*, Vol. 24, No. 8, 1987, pp. 546–551.

[3]Rogers, S. E., Wiltberger, N. L., and Kwak, D., "Efficient Simulation of Incompressible Viscous Flow Over Single and Multi-Element Airfoils," AIAA Paper 92-0405, Jan. 1992.

[4]Rentze, K. J., Buning, P. G., and Rajagopalan, R. G., "A Comparative Study of Turbulence Models for Overset Grids," AIAA Paper 92-0437, Jan. 1992.

[5]Chow, R., and Chu, K., "Navier-Stokes Solution for High-Lift Multielement Airfoil System with Flap Separation," AIAA Paper 91-1623, June 1991.

[6]Mavriplis, D. J., "Euler and Navier-Stokes Computations for Airfoil Geometries Using Unstructured Grids," *CASI Journal*, Vol. 36, No. 2, 1990, pp. 62–71.

[7]Shima, E., "Numerical Analysis of Multiple Element High Lift Devices by Navier-Stokes Equation Using Implicit TVD Finite Volume Method," AIAA Paper 88-2574, June 1988.

[8]Baldwin, B., and Lomax, H., "Thin-Layer Approximation and Algebraic Model for Separated Turbulent Flows," AIAA Paper 78-257, Jan. 1978.

[9]Mavriplis, D. J., "Multigrid Solution of Compressible Turbulent Flow on Unstructured Meshes Using a Two-Equation Model," AIAA Paper 91-0237, Aug. 1991.

[10]Baldwin, B. S., and Barth, T. J., "A One-Equation Turbulence Transport Model for High Reynolds Number Wall-Bounded Flows," NASA TM 102847, Aug. 1990.

[11]Spalart, P. R., and Allamaras, S. R., "A One-Equation Turbulence Model for Aerodynamic Flows," AIAA Paper 92-0439, Jan. 1992.

[12]Squire, L. C., "Interactions Between Wakes and Boundary-Layers," *Progress in Aerospace Sciences*, Vol. 26, 1989, pp. 261–288.

[13]Maksymiuk, C. M., Swanson, R. C., and Pulliam, T. H., "A Comparison of Two Central Difference Schemes for Solving the Navier-Stokes Equations," NASA TM 102815, July 1990.

[14]Yadlin, Y., and Caughey, D. A., "Block Multigrid Implicit Solution of the Euler Equations of Compressible Fluid Flow," *AIAA Journal*, Vol. 29, No. 5, 1991, pp. 712–719.

[15]Nelson, T. E., Zingg, D. W., and Johnston, G. W., "Automated Grid Generation for High-Lift Configurations," *Proceedings of the Third Canadian Symposium on Aerodynamics*, Canadian Aeronautics and Space Institute, Toronto, Nov. 1991.

[16]Pulliam, T. H., "Efficient Solution Methods for the Navier-Stokes Equations," Lecture Notes for the Von Karman Institute for Institute for Fluid Dynamics Lecture Series: *Numerical Techniques for Viscous Flow Computation in Turbomachinery Bladings*, Von Karman Inst. for Fluid Dynamics, Rhone-Saint-Genese, Belgium, Jan. 1986.

[17]Nelson, T. E., Zingg, D. W., and Johnston, G. W., "Numerical Solution of the Navier-Stokes Equations for High-Lift Configurations on Structured Composite Grids," AGARD CP-515, Paper No. 9, Oct. 1992.

[18]Adair, D., and Horne, W. C., "Characteristics of Merging Shear Layers and Turbulent Wakes of a Multi-Element Airfoil," NASA TM 100053, Feb. 1988.

[19]Braden, J. A., Whipkey, R. R., Jones, G. S., and Lilley, D. E., "Experimental Study of the Separating Confluent Boundary-Layer," Vol. I—NASA CR 3655, Vol. II—NASA CR 166018, 1983.

[20] Wentz, W. H., Jr., and Ostowari, C., "Additional Flow Field Studies of the GA(W)-1 Airfoil with 30-Percent Chord Fowler Flap Including Slot-Gap Variations and Cove Shape Modifications," NASA CR-3687, May 1983.